

Large Overall Motion of Flexible Branched Shell Structures

Jacek CHRÓŚCIELEWSKI*, Jerzy MAKOWSKI**, Wojciech PIETRASZKIEWICZ***

**Technical University of Gdańsk, Poland*

***Ruhr University of Bochum, Germany*

****Polish Academy of Sciences, Institute of Fluid-Flow Machinery, Gdańsk, Poland*

Abstract. Within the six-field theory of branched shell structures, a time-stepping algorithm of the non-linear dynamic analysis in the manifold $E^3 \times SO(3)$ is discussed. An indirect C^0 interpolation procedure on $SO(3)$ with a transport of approximation domain is developed. The results of some simulations of the 2D and 3D large motion of the flexible, elastic shell structures are presented.

1. Introduction

Dynamic behaviour of the flexible shell structures undergoing finite deformations and large overall motion has recently gained a considerable interest. We refer to Simo *et al.* [1], Simo and Tarnow [2], Kuhl and Ramm [3], Madeci and Barut [4] and Brank *et al.* [5], where references to other papers are given.

The complete set of field equations as well as initial, boundary and jump conditions describing an arbitrary motion of the irregular shell structures containing folds, branches and/or self-intersections was derived in [6-10] in terms of through-the-thickness resultant quantities. Contrary to a variety of shell models discussed in the literature, the shell relations are exact implications of basic laws of continuum mechanics. The 3D shell is represented by the 2D reference network consisting of a finite number of surface elements joined together along parts of their boundaries. The shell evolution in time is described by two fields defined over the network: the vector field \mathbf{u} representing the translatory motion of the reference network, and the proper orthogonal tensor field \mathbf{Q} representing the mean rotary motion of the shell cross sections. The weak formulation of dynamics of the irregular shell structures based on this shell model is summarised in Section 2.

The aim of this report is to develop for this six-field shell model a time-stepping algorithm for transient dynamic analysis, and to perform some numerical simulations of the behaviour of regular shells and branched, elastic shell structures in forced and free large overall motion.

There are many time-stepping schemes proposed in the literature, where stability and accuracy are most discussed properties of the algorithms. Among recent papers in the non-linear structural dynamics, we refer to Kuhl and Crisfield [11] who discussed several time-stepping algorithms with the properties of numerical dissipation, enforced conservation of energy, algorithmic conservation of energy and combined ones. Similar discussion within the non-linear shell dynamics was given, among others, in Kuhl and Ramm [3]. In our shell model one of the two main independent field variables, $\mathbf{Q} \in SO(3)$,

is an element of the non-linear manifold but not a linear space. As a result, standard time-stepping integrators used in non-linear structural dynamics cannot be directly applied.

The numerical time stepping algorithm used here, in part dealing with the orthogonal group, is based on ideas suggested, among others, by Simo & Vu-Quoc [12], Cardona & Geradin [13] Simo & Wong [14] and Simo and Tarnow [2]. In particular, we take into account that: a) the Newmark integration scheme assures the best possible convergence and stability; b) the angular velocity and the angular acceleration vectors at different time steps can be added directly in the material representation; c) one should try to conserve the energy, the linear and the angular momentum in incremental force-free motion. We use our experience in shell statics [7-9] and propose in the iterative process an exact calculation scheme of the incremental, relative rotation vector. The material representation of this vector plays a crucial role in the time-stepping algorithm.

For spatial discretisation the finite element method is applied. In order to increase the interpolation accuracy for $SO(3)$ -valued fields, we have worked out an accurate, indirect C^0 interpolation procedure with a transport of approximation domain into the neighbourhood of the neutral element $\mathbf{1} \in SO(3)$. Within each finite element the procedure practically removes any singularity following from a local parameterisation, and does not impose any particular parameterisation of \mathcal{Q} . This type of interpolation is of particular importance in dynamical problems of flexible shell structures undergoing large overall motion discussed here. In these problems both the translations and rotations are not bounded at all.

Within the numerical analysis we perform, among others, a standard patch test for a pinched hemisphere with 18° hole. We show that the solution convergence relative to the mesh size decreases rapidly with an increase of the non-linear deformation, the problem which is often ignored. We have also performed several dynamic simulations of the 2D and 3D large overall motions of the flexible, regular and branched, elastic shell structures the results of which are given in Section 6.

2. Weak formulation of dynamics of the irregular shells

Within the general theory of irregular shell structures, the initial (undeformed) configuration of the 3D shell-like body is represented by a 2D surface-like continuum M called briefly an (undeformed) reference network, [9,15]. The network consists of a finite number of surface elements $M^{(k)}, k = 1, 2, \dots, K$ joined together along parts of their boundaries $\partial M^{(k)}$. Each $M^{(k)}$ is a bounded, oriented, connected and smooth surface whose boundaries $\partial M^{(k)}$ consist of a finite number of closed, piecewise smooth curves. Common parts of boundaries of any two or more distinct surface elements form a spatial curve $\Gamma^{(a)}$, and a union of all such curves is called briefly a singular curve $\Gamma \subset M$. Therefore, we have the following definitions:

$$M = \bigcup_{k=1}^K (M^{(k)} \cup \partial M^{(k)}), \quad \partial M = \left(\bigcup_{k=1}^K \partial M^{(k)} \right) \setminus \Gamma, \quad \Gamma = \bigcup_{a=1}^A \Gamma^{(a)}, \quad (2.1)$$

$$\Gamma^{(a)} = \partial M^{(k_1)} \cap \partial M^{(k_2)} \cap \dots \cap \partial M^{(k_m)} \quad \text{if } k_1 \neq k_2 \neq \dots \neq k_m.$$

With each regular point $x \in M$ we can associate the position vector $x \in E^3$ relative to an inertial frame (o, e_i) , where $o \in E^3$ is a point of the 3D Euclidean point space and $e_i \in E^3, i = 1, 2, 3$, are orthonormal vectors. If $(\xi^\alpha), \alpha = 1, 2$, are surface co-ordinates, with

each regular $x \in M$ we can associate the natural surface base vectors and the unit normal vector defined by

$$\mathbf{a}_\alpha = \frac{\partial \mathbf{x}}{\partial \xi^\alpha} \equiv \mathbf{x}_{,\alpha}, \quad \mathbf{a}^\beta \cdot \mathbf{a}_\alpha = \delta_\alpha^\beta, \quad \mathbf{a}_3 = \frac{1}{2} \epsilon^{\alpha\beta} \mathbf{a}_\alpha \times \mathbf{a}_\beta, \quad (2.2)$$

where $\epsilon^{\alpha\beta}$ are surface permutation symbols.

The motion of the shell in time t can be described by two fields defined over the reference network: the position vector field $\mathbf{y}(\mathbf{x}, t)$ representing the translatory motion of the shell reference network, and the proper orthogonal tensor field $\mathbf{Q}(\mathbf{x}, t)$ representing the mean rotary motion of the shell cross sections.

The general mechanical theory of irregular shell structures was developed in [8,9]. Within this approach the 2D balance equations of translational and rotational momentum, the dynamical boundary and jump conditions, the kinematic relations, the kinematic boundary and jump conditions, and the initial conditions are exact consequences of the corresponding relations of continuum mechanics. Unavoidable approximations enter the shell theory only through kinematic and material constitutive relations. We refer the reader to papers mentioned above and to Chróscielewski *et al.* [7] and Libai and Simmonds [10] for details of the derivation process, necessary regularity assumptions for all the fields and references to other papers.

In this report we confine ourselves only to geometric irregularities and allow the shell to have only folds, branches and/or self-intersections. We assume from the beginning that the kinematic fields $\mathbf{y}(\mathbf{x}, t)$ and $\mathbf{Q}(\mathbf{x}, t)$ are continuous during the motion, and $\mathbf{y}_\Gamma(\mathbf{x}_\Gamma, t) = \mathbf{y}(\mathbf{x}, t)|_\Gamma$, $\mathbf{Q}_\Gamma(\mathbf{x}_\Gamma, t) = \mathbf{Q}(\mathbf{x}, t)|_\Gamma$, with $\mathbf{x}_\Gamma \in \Gamma$. We do not associate here any mechanical properties with the singular curve Γ as well.

When expressed in the weak form, the initial-boundary value problem (IBVP) for the irregular shell-like structure can be formulated as follows: Given the external resultant force and couple vector fields $\mathbf{f}(\mathbf{x}, t)$ and $\mathbf{c}(\mathbf{x}, t)$ on $\mathbf{x} \in M \setminus \Gamma$, $\mathbf{n}^*(\mathbf{x}, t)$ and $\mathbf{m}^*(\mathbf{x}, t)$ along ∂M_f , $\mathbf{n}_\Gamma(\mathbf{x}, t)$ and $\mathbf{m}_\Gamma(\mathbf{x}, t)$ along the singular curve $\Gamma \subset M$, and the initial values $\mathbf{u}_0(\mathbf{x})$, $\mathbf{Q}_0(\mathbf{x})$, $\dot{\mathbf{u}}_0(\mathbf{x})$, $\dot{\mathbf{Q}}_0(\mathbf{x})$ at $t=0$ find a curve $\mathbb{w}(\mathbf{x}, t) = (\mathbf{u}(\mathbf{x}, t), \mathbf{Q}(\mathbf{x}, t))$ on the configuration space $C(M, E^3 \times SO(3))$ such that for any continuous, kinematically admissible virtual vector fields $(\mathbf{v}(\mathbf{x}), \mathbf{w}(\mathbf{x})) \equiv \delta \mathbb{w}(\mathbf{x}) \in V_A(M, E^3 \times E^3)$ we have

$$\begin{aligned} G[\mathbb{w}; \delta \mathbb{w}] = & \iint_{M \setminus \Gamma} [\dot{\mathbf{p}} \cdot \mathbf{v} + (\dot{\mathbf{m}} + \mathbf{v} \times \mathbf{p}) \cdot \mathbf{w}] da + \iint_{M \setminus \Gamma} [\mathbf{n}^\beta \cdot (\mathbf{v}_{,\beta} + \mathbf{y}_{,\beta} \times \mathbf{w}) + \mathbf{m}^\beta \cdot \mathbf{w}_{,\beta}] da \\ & - \iint_{M \setminus \Gamma} (\mathbf{f} \cdot \mathbf{v} + \mathbf{c} \cdot \mathbf{w}) da - \int_{\partial M_f} (\mathbf{n}^* \cdot \mathbf{v} + \mathbf{m}^* \cdot \mathbf{w}) ds - \int_\Gamma (\mathbf{p}_\Gamma \cdot \mathbf{v}_\Gamma + \mathbf{m}_\Gamma \cdot \mathbf{w}_\Gamma) ds = 0. \end{aligned} \quad (2.3)$$

Here $\mathbf{u}(\mathbf{x}, t) = \mathbf{y}(\mathbf{x}, t) - \mathbf{x}$ is the network displacement vector, $\mathbf{v}(\mathbf{x}, t) = \dot{\mathbf{y}}(\mathbf{x}, t) = \dot{\mathbf{u}}(\mathbf{x}, t)$ is the network velocity vector, $\mathbf{p}(\mathbf{x}, t)$ and $\mathbf{m}(\mathbf{x}, t)$ are the translational and rotational momenta vectors, $\mathbf{n}^\beta(\mathbf{x}, t)$ and $\mathbf{m}^\beta(\mathbf{x}, t)$ are the internal stress and couple resultant vectors, respectively, and $\mathbf{v}_\Gamma = \mathbf{v}|_\Gamma$, $\mathbf{w}_\Gamma = \mathbf{w}|_\Gamma$. In (2.3) it is implicitly assumed that the kinematic boundary conditions $\mathbf{u}(\mathbf{x}, t) = \mathbf{u}^*(\mathbf{x}, t)$ and $\mathbf{Q}(\mathbf{x}, t) = \mathbf{Q}^*(\mathbf{x}, t)$ are satisfied on the complementary part $\partial M_d = \partial M \setminus \partial M_f$, and the virtual vector fields are admissible if $\mathbf{v}(\mathbf{x}) = \mathbf{0}$ and $\mathbf{w}(\mathbf{x}) = \mathbf{0}$ on ∂M_d .

In the shell theory the explicit expressions for the momenta \mathbf{p} and \mathbf{m} should be specified by the kinematic constitutive relations, in general. In this report we shall use simple relations suggested in [10]:

$$\mathbf{p} = \rho_0 h_0 \mathbf{v}, \quad \mathbf{m} = (\rho_0 h_0^3 / 12) \boldsymbol{\omega}, \quad \boldsymbol{\omega} \times \mathbf{1} = \dot{\mathbf{Q}} \mathbf{Q}^T, \quad (2.4)$$

where $\rho_0(\mathbf{x})$ is the initial mass density, $h_0(\mathbf{x})$ is the initial shell thickness, and $\boldsymbol{\omega}(\mathbf{x}, t)$ is the network spin vector in the spatial representation.

The resultants \mathbf{n}^β and \mathbf{m}^β should be given through the constitutive relations of the material the shell is composed of. In this report we restrict our interest to the hyper-elastic shells for which there exists a 2D strain energy function $W(\boldsymbol{\varepsilon}_\beta, \boldsymbol{\kappa}_\beta; \mathbf{x})$ of the shell strain vectors which are defined by

$$\boldsymbol{\varepsilon}_\beta = \mathbf{y}_{,\beta} - \mathbf{a}_\beta, \quad \boldsymbol{\kappa}_\beta \times \mathbf{1} = \mathbf{Q}_{,\beta} \mathbf{Q}^T. \quad (2.5)$$

Then the constitutive relations are given by

$$\mathbf{n}^\beta = \partial W / \partial \boldsymbol{\varepsilon}_\beta, \quad \mathbf{m}^\beta = \partial W / \partial \boldsymbol{\kappa}_\beta. \quad (2.6)$$

The solution of the non-linear IBVP (2.3) is achieved by an iterative procedure which reduces the problem to a sequence of solutions of linearised problems. Each linearised problem is formulated at discrete values of both temporal and spatial variables. The main difficulty of the solution procedure is associated with the structure of the configuration space $C(M, E^3 \times SO(3))$ involving the proper orthogonal group $SO(3)$. As a result, the solution procedure requires special techniques for approximation, parameterisation, interpolation, and accumulation of the $SO(3)$ -valued fields.

3. Time-stepping algorithm

Let the time interval $[0, T]$ be partitioned by a finite number of time instants $0 < t_1 < t_2 < \dots < t_n < t_{n+1} < \dots < T$ such that $[0, T] = \bigcup_{n=1}^N [t_n, t_{n+1}]$. Denote values at the typical time instant t_n of the generalised displacements \mathbb{w} , velocities $\mathbb{v} = (\mathbf{v}, \boldsymbol{\omega}) = (\mathbf{v}, \mathbf{Q}^T \boldsymbol{\omega})$ and accelerations $\mathbb{a} = (\dot{\mathbf{v}}, \dot{\boldsymbol{\omega}}) = (\dot{\mathbf{v}}, \mathbf{Q}^T \dot{\boldsymbol{\omega}})$ in the material representation by

$$\mathbb{w}_n = \mathbb{w}(t_n) \in C_A, \quad \mathbb{v}_n = \mathbb{v}(t_n) \in V_A, \quad \mathbb{a}_n = \mathbb{a}(t_n) \in V_A. \quad (3.1)$$

Assuming the data (3.1) be given up to time t_n , the objective of various time-stepping algorithms is to find at the next time instant $t_{n+1} = t_n + \Delta t$ a consistent and stable approximations $\mathbb{w}_{n+1}, \mathbb{v}_{n+1}, \mathbb{a}_{n+1}$ to the actual values $\mathbb{w}(t_{n+1}), \mathbb{v}(t_{n+1}), \mathbb{a}(t_{n+1})$.

There are many time-stepping algorithms proposed in the literature for solving dynamical problems in the linear space. Among engineers the most popular are those based on the one-step Newmark [16] formula in which the actual state at time t_{n+1} is calculated from the former state at time t_n alone. In case of the non-linear shell dynamics discussed here the configuration space C does not have the structure of the linear space. In this case essential difficulties arise in the extension of classical time-stepping algorithms to hold in C . Several extensions of the Newmark formula to the rotation group $SO(3)$ were proposed

e.g. in [12-14,2]. In the extensions the concepts of differential geometry such as exponential map and parallel transport play the important role.

In general, the weak form of the IBVP at the time instant t_{n+1} can be written as

$$G[\mathbb{w}_{n+1}; \delta \mathbb{w}] = 0, \quad \forall \delta \mathbb{w} \in V_A, \quad (3.2)$$

for the unknown generalised displacement $\mathbb{w}_{n+1} \in C$.

In the non-linear computational dynamics the main interest is focused on numerical stability of the time integrators. It is known that unconditionally stable algorithms of linear dynamics often lose this property in problems of non-linear dynamics. In the latter case a sufficient condition for some kind of stability is the conservation or decay of the total energy within a time step. When analysing free motion of the body, the energy, the linear momentum as well as the angular momentum must be conserved. These requirements form the general basis for the formulation of various time integrators.

Time-stepping algorithms for non-linear dynamical problems involving large overall motions can be characterised by three main features: a) numerical dissipation, b) enforced conservation of energy and momenta, and c) algorithmic conservation of energy and momenta. The time integration code used in this report has been so constructed that all the three features can be discussed by changing values of some parameters.

After Chung and Hulbert [17] we introduce into the extended Newmark scheme two scalar parameters $0 \leq \alpha_m \leq 1$ and $0 \leq \alpha_f \leq 1$ responsible for modelling the numerical dissipation. We also use discrete time combinations of the generalised accelerations, velocities, displacements and of the external generalised forces according to the scheme

$$\begin{aligned} \mathfrak{a}_{n+1-\alpha_m} &= (1 - \alpha_m) \mathfrak{a}_{n+1} + \alpha_m \mathfrak{a}_n, \\ \mathfrak{v}_{n+1-\alpha_f} &= (1 - \alpha_f) \mathfrak{v}_{n+1} + \alpha_f \mathfrak{v}_n, \\ \mathbb{w}_{n+1-\alpha_f} &= (1 - \alpha_f) \mathbb{w}_{n+1} \oplus \alpha_f \mathbb{w}_n, \\ \mathfrak{f}_{n+1-\alpha_f} &= (1 - \alpha_f) \mathfrak{f}_{n+1} + \alpha_f \mathfrak{f}_n. \end{aligned} \quad (3.3)$$

Here the subscripts $n+1-\alpha_m$ and $n+1-\alpha_f$ indicate that these variables are given at a mid point of the time step, depending of the values taken for α_m and α_f . All the operations performed in (3.3)₁₋₃ are understood to be taken for components relative to the same base. This means, in particular, that for the rotational part of \mathfrak{v} and \mathfrak{a} these operations make sense only in the material representation. The symbol \oplus is understood as the accumulation of the generalised displacements $\mathbb{w} = (\mathbf{u}, \mathbf{Q}) \in (E^3 \times SO(3))$, while the symbol \mathfrak{f} means here any of the external load vectors. The internal resultant forces $\mathfrak{m} = (\mathbf{n}^\beta, \mathbf{m}^\beta)$ of the P-K type are given at the mid-point $n+1-\alpha_f$ classically as

$$\mathfrak{m}_{n+1-\alpha_f} = (1 - \alpha_f) \mathfrak{m}_{n+1} + \alpha_f \mathfrak{m}_n. \quad (3.4)$$

Alternatively, we can use the algorithmic form

$$\mathfrak{m}_{n+1-\alpha_f} = \mathfrak{m}(\mathbb{w}_{n+1-f}), \quad (3.5)$$

depending of the time integration scheme applied. When applying the generalised energy-momentum method, $\mathfrak{m}_{n+1-\alpha_f}$ are expressed by the linear constitutive equations of elasticity in terms of the generalised strains $\mathfrak{e} = (\boldsymbol{\varepsilon}_\beta, \boldsymbol{\kappa}_\beta)$, for which the following scheme is used

$$\mathbf{e}_{n+1-\alpha_f} = (1 - \alpha_f)\mathbf{e}_{n+1} + \alpha_f\mathbf{e}_n. \quad (3.6)$$

With $\alpha_m = \alpha_f = 0.5$ this case reduces to Simo and Tarnow [2] method.

With (3.3) and the standard Newmark formula, for the generalised accelerations and velocities at the mid-point we obtain

$$\begin{aligned} \bar{\mathbf{a}}_{n+1-\alpha_m} &= \frac{1 - \alpha_m}{\beta(\Delta t)^2} \Delta \mathbb{w} - \frac{1 - \alpha_m}{\beta \Delta t} \mathbb{v}_n - \frac{1 - \alpha_m - 2\beta}{2\beta} \bar{\mathbf{a}}_n, \\ \mathbb{v}_{n+1-\alpha_f} &= \frac{\gamma(1 - \alpha_f)}{\beta \Delta t} \Delta \mathbb{w} - \frac{\gamma(1 - \alpha_f) - \beta}{\beta} \mathbb{v}_n - \Delta t \frac{(\gamma - 2\beta)(1 - \alpha_f)}{2\beta} \bar{\mathbf{a}}_n. \end{aligned} \quad (3.7)$$

Here $\Delta \mathbb{w} = (\Delta \mathbf{u}, \Delta \boldsymbol{\theta})$, $\Delta \mathbf{u} = \mathbf{u}_{n+1} - \mathbf{u}_n$, $\Delta \boldsymbol{\theta}$ is defined by the relations $\Delta \mathbf{Q} = \exp(\Delta \boldsymbol{\theta} \times \mathbf{1})$, $\mathbf{Q}_{n+1} = \mathbf{Q}_n \Delta \mathbf{Q}$, and $0 \leq \beta \leq 0.5$ and $0 \leq \gamma \leq 1$ are parameters of the Newmark algorithm.

Specialisation of the parameters α_m , α_f , β and γ leads to a variety of known time integration schemes and their extensions for $E^3 \times SO(3)$.

4. Iterative solution of the non-linear problem

The solution of the non-linear problem (3.2) is constructed by the iterative procedure based on the standard Newton-Kantorovich method [20] applied in the configuration space $C(M, E^3 \times SO(3))$. Let an i -th approximation $\mathbb{w}_{n+1}^{(i)}$ to the solution \mathbb{w}_{n+1} has been found. In order to calculate the correction $\Delta \mathbb{w}_{n+1}^{(i)}$, which would allow us to calculate the successive approximation $\mathbb{w}_{n+1}^{(i+1)} = \mathbb{w}_{n+1}^{(i)} \oplus \Delta \mathbb{w}_{n+1}^{(i)}$ to the unknown solution \mathbb{w}_{n+1} , we linearise $G[\mathbb{w}_{n+1}; \delta \mathbb{w}]$ at the approximation $\mathbb{w}_{n+1}^{(i)}$:

$$G[\mathbb{w}_{n+1}^{(i)}; \delta \mathbb{w}] + \delta G[\mathbb{w}_{n+1}^{(i)}, \Delta \mathbb{w}_{n+1}^{(i)}; \delta \mathbb{w}] = 0. \quad (4.1)$$

The second term in (4.1) denotes a directional derivative of the functional $G[\mathbb{w}_{n+1}; \delta \mathbb{w}]$, taken at the point $\mathbb{w}_{n+1}^{(i)} \in C$ in the kinematically admissible direction $\Delta \mathbb{w}_{n+1}^{(i)} \in T_{\mathbb{w}_{n+1}^{(i)}} C$. This term yields the so-called tangent operator of the non-linear problem, calculated at the approximation $\mathbb{w}_{n+1}^{(i)}$. The first term in (4.1) represents the unbalanced forces at the approximation point $\mathbb{w}_{n+1}^{(i)}$.

In the case of the constrained energy momentum algorithm [3], the basic functional (2.3) should be extended by adding explicitly the balance laws of the energy, the linear momentum and the angular momentum with corresponding seven Lagrange multipliers $\boldsymbol{\lambda}$. Then the linearisation formula (4.1) for the corresponding extended functional $G[\mathbb{w}, \boldsymbol{\lambda}; \delta \mathbb{w}, \delta \boldsymbol{\lambda}]$ should be understood as taken in the extended configuration space.

5. Spatial discretisation and interpolation in $SO(3)$

The main advantage of the mechanical theory of irregular shell structures discussed in the previous sections is that only C^0 continuity requirement is imposed upon the primary kinematic field $\mathbb{w} = (\mathbf{u}, \mathbf{Q})$. When applying the finite element method we proceed as follows.

The shell reference network M (the domain) is divided into sub-domains $\Pi_{(e)}$, $e = 1, 2, \dots, E$, (finite elements) such that $M = \bigcup_{e=1}^E \Pi_{(e)}$. A typical finite element $\Pi_{(e)}$ is a smooth image of a compact, bounded region $\pi_{(e)} \in R^2$, usually a triangle or a rectangle. Let $\boldsymbol{\eta} = (\eta_1, \eta_2)$ be local co-ordinates of $\pi_{(e)}$, $\Delta = \{\boldsymbol{\eta}_a \in \pi_{(e)}, a = 1, 2, \dots, A\}$ be a set of A distinct points of $\pi_{(e)}$ called the nodes, $\mathbb{W}(\boldsymbol{\eta}) = (\mathbf{u}(\boldsymbol{\eta}), \mathbf{Q}(\boldsymbol{\eta})) \in C(\pi_{(e)}, E^3 \times SO(3))$ be a given smooth function on $\pi_{(e)}$ with values in the six-dimensional Lie group $E^3 \times SO(3)$, and let $\mathbb{W}_a = (\mathbf{u}_a, \mathbf{Q}_a) = (\mathbf{u}(\boldsymbol{\eta}_a), \mathbf{Q}(\boldsymbol{\eta}_a))$ denote values of \mathbb{W} at the nodes $\boldsymbol{\eta}_a$. Within each $\pi_{(e)}$ we have to construct an approximating function $\tilde{\mathbb{W}}(\boldsymbol{\eta}) = (\tilde{\mathbf{u}}(\boldsymbol{\eta}), \tilde{\mathbf{Q}}(\boldsymbol{\eta}))$ which takes the same values at the nodes $\boldsymbol{\eta}_a$ as \mathbb{W} does (that is $\tilde{\mathbb{W}}(\boldsymbol{\eta}_a) = \mathbb{W}_a$ for any $\boldsymbol{\eta}_a \in \Delta$) and is “close” - in some defined sense - to the given function $\mathbb{W}(\boldsymbol{\eta})$.

The standard C^0 interpolation of the E^3 -valued function $\mathbf{u}(\boldsymbol{\eta})$ at the nodes $\boldsymbol{\eta}_a$ takes the form

$$\tilde{\mathbf{u}}(\boldsymbol{\eta}) = \sum_{a=1}^A N_a(\boldsymbol{\eta}) \mathbf{u}_a, \quad (5.1)$$

where $N_a(\boldsymbol{\eta})$ are given shape functions (usually products of the Lagrange polynomials, see Zienkiewicz [18]) satisfying the conditions $N_a(\boldsymbol{\eta}_b) = \delta_{ab}$ for any $\boldsymbol{\eta}_b \in \Delta$.

For the $SO(3)$ -valued function such a standard, canonical interpolation scheme is not available. We proposed in [7] a kind of indirect C^0 interpolation procedure on $SO(3)$ through interpolation of three scalar functions $\vartheta_k(\boldsymbol{\eta})$ of local parameters. Numerical test examples presented in [19] indicate, however, that the procedure leads to a decrease of interpolation accuracy away from the neutral element $\mathbf{1} \in SO(3)$. Here we propose a modified, free from such a defect, indirect C^0 interpolation procedure on $SO(3)$ with a transport of approximation domain into the neighbourhood of the neutral element $\mathbf{1} \in SO(3)$.

Let a local parameterisation of the rotation group be given by

$$\mathbf{Q} \xrightarrow{\quad} (\vartheta_k), \quad (5.2)$$

where $\mathbf{Q} \in U \subset SO(3)$ and $(\vartheta_k) = \mathbf{D}(\mathbf{Q}) \in V \subset R^3$, $k = 1, 2, 3$, are three chosen, independent local parameters, and $\mathbf{Q}(\boldsymbol{\eta}) = \mathbf{I}^{-1}(\vartheta_k(\boldsymbol{\eta}))$. The modified interpolation procedure on $SO(3)$ consists of the following steps:

1. Establishing for the set of nodal tensors $\mathbf{Q}_a = \mathbf{Q}(\boldsymbol{\eta}_a) \in U \subset SO(3)$ a constant, averaged representative $\bar{\mathbf{Q}} \in SO(3)$.
2. Transporting the set \mathbf{Q}_a by the kind of pull-back with $\bar{\mathbf{Q}}^T: U \rightarrow W \subset SO(3)$ into the “neighbourhood” of $\mathbf{1} \in W \subset SO(3)$:

$$\mathbf{R}_a = \bar{\mathbf{Q}}^T \mathbf{Q}_a. \quad (5.3)$$

3. Introducing three local parameters in the map (W, \mathbf{J}) for the transported tensor field:

$$(\rho_k)_a = \mathbf{J}(\mathbf{R}_a). \quad (5.4)$$

4. Interpolating the scalar functions $\rho_k(\boldsymbol{\eta}) \in R^3$ through the nodal values $(\rho_k)_a$ according to the scheme (5.1):

$$\tilde{\rho}(\boldsymbol{\eta}) = \sum_{a=1}^A N_a(\boldsymbol{\eta}) \rho_a. \quad (5.5)$$

5. Calculating the interpolating tensor function $\tilde{\mathbf{R}}(\boldsymbol{\eta})$:

$$\tilde{\mathbf{R}}(\boldsymbol{\eta}) = \mathbf{J}^{-1}(\tilde{\rho}(\boldsymbol{\eta})). \quad (5.6)$$

6. Transporting back the function $\tilde{\mathbf{R}}(\boldsymbol{\eta})$ into the initial position in $SO(3)$ by the kind of push-forward with $\bar{\mathbf{Q}}:W \rightarrow U \subset SO(3)$:

$$\tilde{\mathbf{Q}}(\boldsymbol{\eta}) = \bar{\mathbf{Q}}\tilde{\mathbf{R}}(\boldsymbol{\eta}). \quad (5.7)$$

Therefore, $\tilde{\mathbf{Q}}(\boldsymbol{\eta})$ interpolates the given function $\mathbf{Q}(\boldsymbol{\eta}) \in C(\pi_{(e)}, SO(3))$ at the set of nodes $\boldsymbol{\eta}_a \in \Delta$ indeed. From (5.7) it also follows that the interpolating function $\tilde{\mathbf{Q}}(\boldsymbol{\eta})$ always takes values in the rotation group. Within each finite element the proposed interpolation procedure practically removes any singularity which may follow from a local parameterisation. The procedure itself does not impose any particular parameterisation of \mathbf{Q} . As a result, it can be used for any non-singular global parameterisation of the rotation group $SO(3)$.

In the incremental-iterative procedure described in Section 4 the fields of incremental rotation vector $\Delta\boldsymbol{\psi} \times \mathbf{1} = \Delta\mathbf{Q}\mathbf{Q}^T$ and the virtual rotation vector $\delta\boldsymbol{\psi} \times \mathbf{1} = \delta\mathbf{Q}\mathbf{Q}^T$ play a different role than the field of rotation tensor \mathbf{Q} itself. In the numerical procedure the fields $\Delta\boldsymbol{\psi}$ and $\boldsymbol{\psi}$ appear as the ‘‘unknown’’ ones. If they are expressed through the incremental $\Delta\vartheta_k$ and virtual $\delta\vartheta_k$ local parameters of the tensor field \mathbf{Q} , respectively, the C^0 interelement continuity requirement is transferred to the chosen parameterisation. The necessity to fulfil continuity of the local parameters restricts applicability of the algorithm to problems contained in only one local map (U, l) . For a curved shell structure, and for dynamic problems in particular, this decreases the interpolation accuracy as well, [19].

The virtual rotation $\delta\mathbf{Q}$ at the regular $\mathbf{Q} \in C(\pi_{(e)}, SO(3))$ is an element of the tangent space $T_{\mathbf{Q}}C(\pi_{(e)}, SO(3)) \approx C(\pi_{(e)}, T_{\mathbf{Q}}SO(3))$, where \approx indicates an isomorphism. We also have further isomorphisms of spaces $T_{\mathbf{Q}}C(\pi_{(e)}, SO(3)) \approx C(\pi_{(e)}, so(3)) \approx C(\pi_{(e)}, E^3)$ and their elements $\delta\mathbf{Q} \rightarrow \boldsymbol{\Psi} \rightarrow \boldsymbol{\psi}$, where $\boldsymbol{\Psi} = \delta\mathbf{Q}\mathbf{Q}^T = \boldsymbol{\psi} \times \mathbf{1}$ is the skew-symmetric tensor having $\boldsymbol{\psi}$ as the axial vector.

The virtual rotation vector $\boldsymbol{\psi}$ can be represented through components either in the co-rotating \mathbf{d}_i or in the fixed, global \mathbf{e}_i bases. If $\mathbf{d}_i = \mathbf{T}\mathbf{e}_i = T_{ij}\mathbf{e}_j$, where $\mathbf{T} \in SO(3)$, then

$$\boldsymbol{\psi} = \psi_i \mathbf{d}_i = \bar{\psi}_j \mathbf{e}_j = \bar{\psi}_j T_{ij} \mathbf{d}_i, \quad (5.8)$$

where the corresponding components are related by $\psi_i = T_{ij} \bar{\psi}_j$. With (5.8) we obtain the matrix form of the interpolation formula

$$\begin{Bmatrix} \tilde{\psi}_1(\boldsymbol{\eta}) \\ \tilde{\psi}_2(\boldsymbol{\eta}) \\ \tilde{\psi}_3(\boldsymbol{\eta}) \end{Bmatrix} = \mathbb{T}(\boldsymbol{\eta}) \sum_{a=1}^A N_a(\boldsymbol{\eta}) \begin{Bmatrix} \bar{\psi}_{1a} \\ \bar{\psi}_{2a} \\ \bar{\psi}_{3a} \end{Bmatrix}, \quad \mathbb{T}(\boldsymbol{\eta}) : \begin{Bmatrix} \bar{\psi}_1(\boldsymbol{\eta}) \\ \bar{\psi}_2(\boldsymbol{\eta}) \\ \bar{\psi}_3(\boldsymbol{\eta}) \end{Bmatrix} \rightarrow \begin{Bmatrix} \psi_1(\boldsymbol{\eta}) \\ \psi_2(\boldsymbol{\eta}) \\ \psi_3(\boldsymbol{\eta}) \end{Bmatrix}. \quad (5.9)$$

Components of the nodal parameters $\bar{\psi}_{ia}$ are given in the global, fixed base e_i common to all the elements and the nodes. This allows one to describe easily the junctions of different branches $M^{(k)}$ of M . The components $\bar{\psi}_{ia}$ and ψ_{ia} can easily be expressed in terms of nodal displacements which provides an engineering interpretation to these components.

6. Numerical simulations

6.1. Free-free flexible beam undergoing large overall motion

This problem was analysed in several papers on beam dynamics in 2D and 3D formulation, for example in [12] using the rod model. The beam initially at an inclined position in the plane (e_1, e_3) is loaded at the lower end by a spatially fixed force P and torque M with components and time histories as in Fig. 6.1.

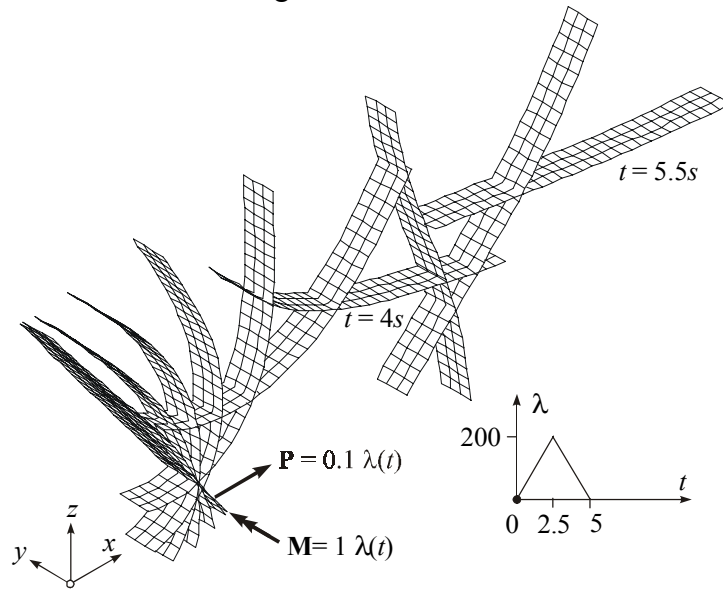


Fig. 6.1. 3D view of some configurations of the flexible beam in 2D free motion

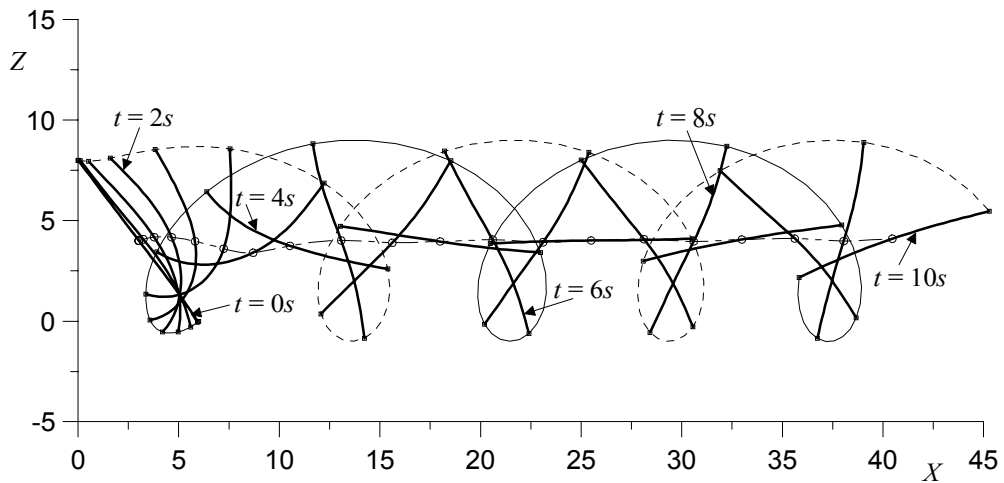


Fig. 6.2. Deformation history of the free-free flexible beam undergoing large overall 2D motion

We solve here the same problem using the six-field shell model with the following data: $L = 10$, $L_x = 6$, $L_y = 8$, $b = h_0 = 1$, $EA = 10^4$, $EJ = Ebh_0^3/12 = 500$, $\rho_0 A = 1$, $\rho_0 J = 10$.

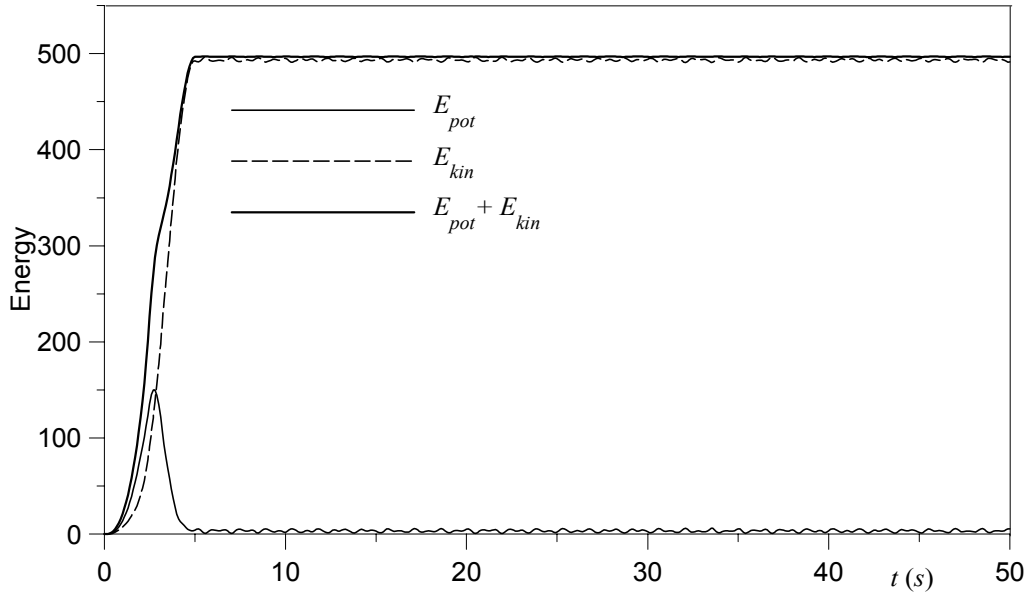


Fig. 6.3. Energy history plots for the 2D free motion of the flexible beam

The deformation history of plane configurations of the beam is given in Fig. 6.2, while the sequence of plane configurations as seen from 3D perspective is shown in Fig. 6.1. Plots of energies depicted in Fig. 6.3 indicate small oscillations of the kinetic and potential energies, but the total energy remains constant in time. Our results confirm the dynamical behaviour of the rod discussed in other papers.

6.2. Free-free flexible beam undergoing rotary motion

To verify the importance of the sixth degree of freedom (drilling rotation) in shell dynamics we analyse the rotary motion of the free-free beam under the action of the external couple applied at the centre C of the beam, Fig. 6.4. Two solutions – based on shell theory, and based on plane-stress elasticity (membrane) – are compared in 2D rotary motion. The data characteristics relative to the previous example are united: $L = L_x = 10$, $b = h_0 = 1$, $E = 10^4$, $\nu = 0$, and $\rho_0 = 1$. Please note that the couple applied at the central point C is here

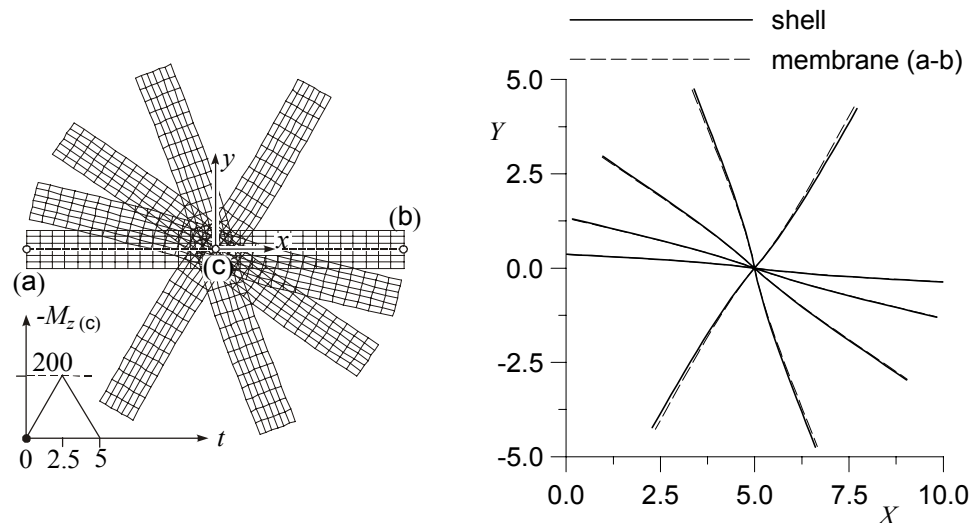


Fig. 6.4. The comparison of the shell and the membrane solutions

the drilling couple. Such an example cannot be analysed by other shell models without an independent sixth degree of freedom. In this example the shell theory gives similar results as the membrane solution.

6.3. Free-free thin strip powered by two couples

By reducing 100 times the thickness of the beam from the previous example, we discuss the dynamic behaviour of the thin strip with data $L = L_x = 10$, $b = 1$, $h_0 = 0.01$, $E = 10^4$, $\nu = 0.25$, $\rho_0 = 1$. The strip is powered by two dynamically applied couples: the couple $M_x(t)$ acting along the strip axis, and a small perturbing couple $M_y(t) = 0.05M_x(t)$, Fig. 6.5. The problem illustrates the loss of dynamic stability of the strip about the X axis. Several spatial post-buckling configurations at successive time instants are shown in Fig. 6.5, while Fig. 6.6 indicates the trajectories of the two end points (a) and (b) projected onto the $Y - Z$ co-ordinate plane.

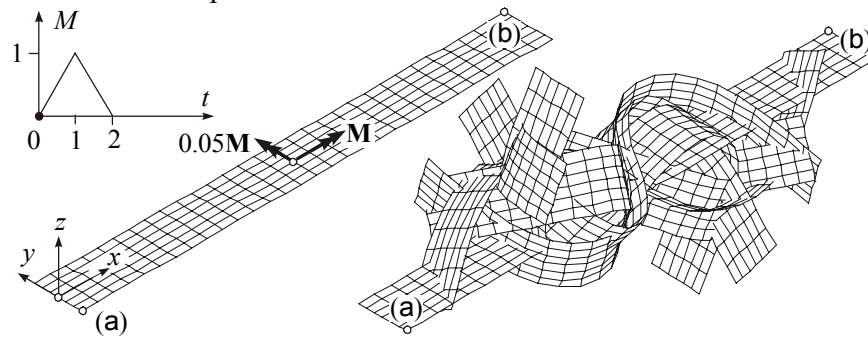


Fig. 6.5. Free-free thin strip powered by two couples: couple application data and spatial configurations of the strip at successive time instants

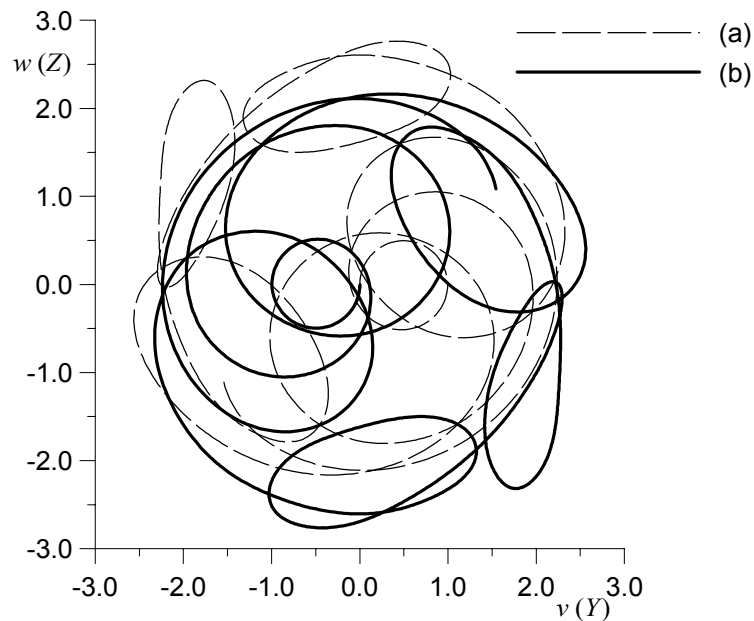


Fig. 6.6. Trajectories of the end points (a) and (b)

6.4. Right-angle cantilever beam subjected to an out-of-plane force

This problem was analysed by beam models in many papers, in particular by Simo and Vu-Quoc [12]. The right-angle cantilever beam is subjected to an out-of-plane concentrated force applied at the elbow (a) by a hat time function, Fig. 6.7.

In our example solved by the shell model we take the data $L_x=L_y=10$, $b=h_0=(12/10^3)^{1/2}$, $E=10^9/12$, $\nu=0$, $\rho_0=10^3/12$ in order to obtain the same sectional characteristics $EA=10^6$, $\rho_0A=1$, $EJ=10^3$ as in the examples based on the beam theory. However, our torsional stiffness and rotary inertia are different from those used in earlier beam papers. Therefore, our results are not comparable to earlier beam results.

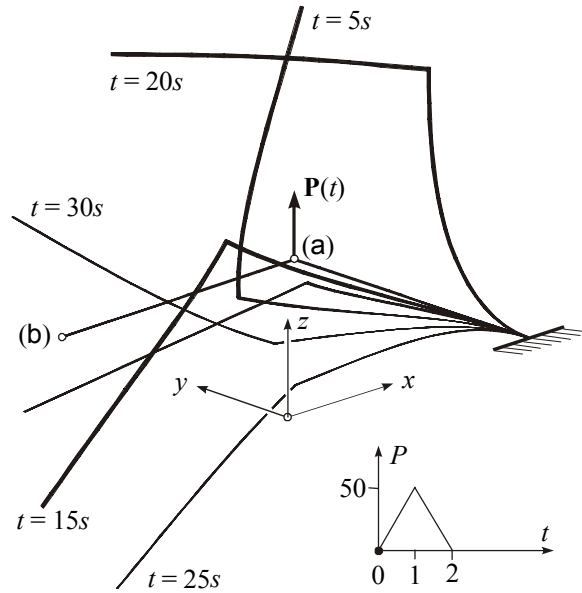


Fig. 6.7. Right-angle cantilever beam: the applied force data and deformed configurations at five time instants

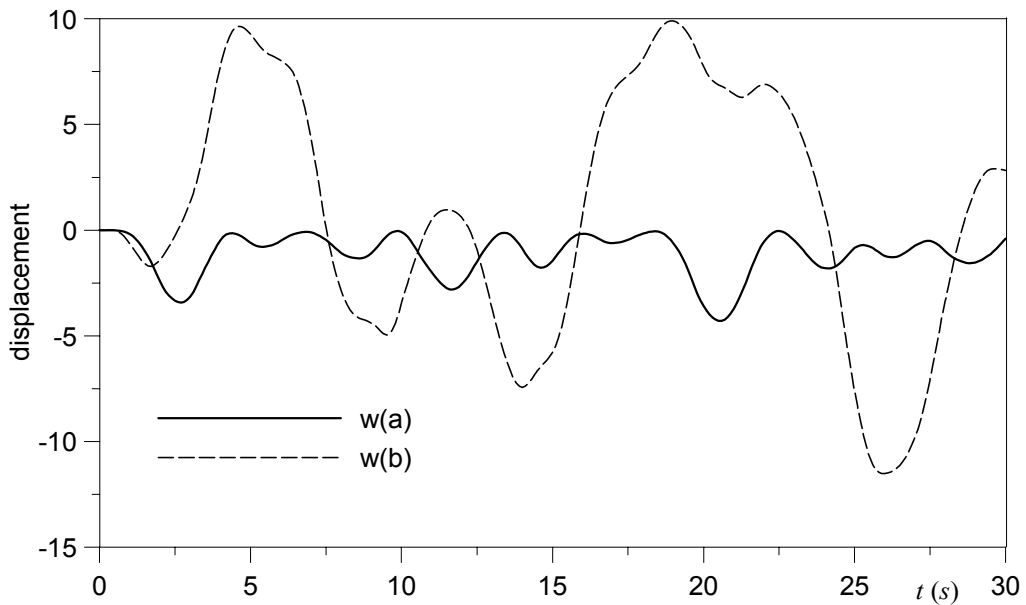


Fig. 6.8. Time histories of out-of-plane displacements of the points (a) and (b)

The cantilever is discretised into 44 9-nodes elements with full integration 3×3 . After removal of the force the cantilever undergoes finite free vibrations with combined bending and torsion. The time histories of the out-of-plane displacement of the points (a) and (b) are given in Fig. 6.8. While the values of potential and kinetic energies oscillate in a wide range, Fig. 6.9, the total energy remains almost constant in time.

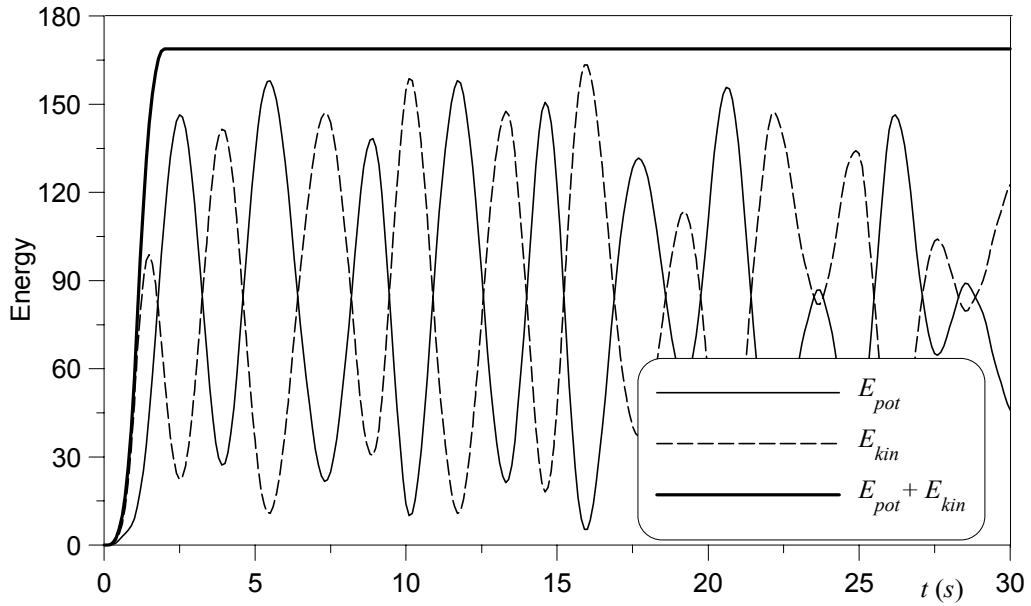
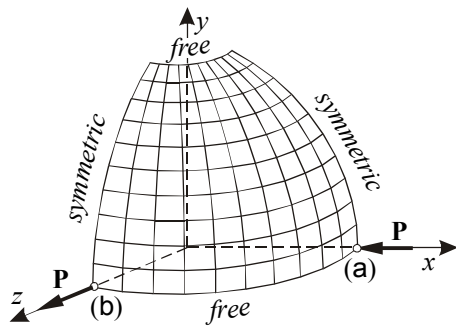


Fig. 6.9. Energy histories for non-linear vibrations of the right-angle cantilever beam

6.5. The hemisphere with an 18° hole



We solve first the equilibrium problem for the octant panel of the hemisphere with an 18° hole, which is subjected to the self-equilibrated two inward and outward forces applied at the base edges, Fig. 6.10. The problem with the data $R=10$, $h_0=0.04$, $\alpha=18^\circ$, $E=6.825 \times 10^7$, $\nu=0.3$, $P=\lambda P_{ref}$, $P_{ref}=10$ is often used as a solution convergence test for finite elements.

Fig. 6.10. The octant panel of the hemisphere: the geometry and the applied loading

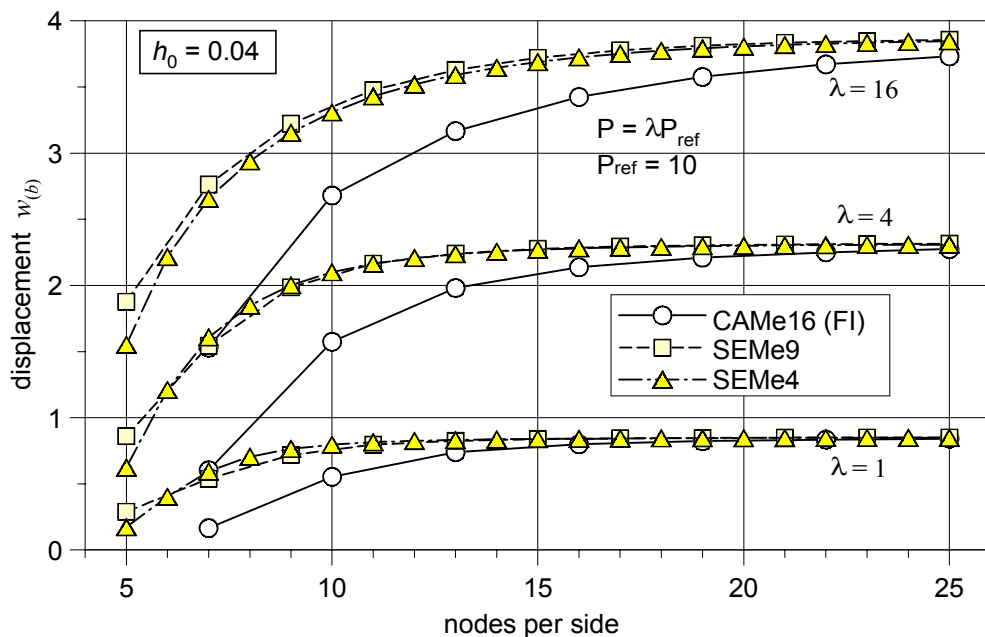


Fig. 6.11. The hemisphere with the hole: the slower rate of convergence with increasing load level

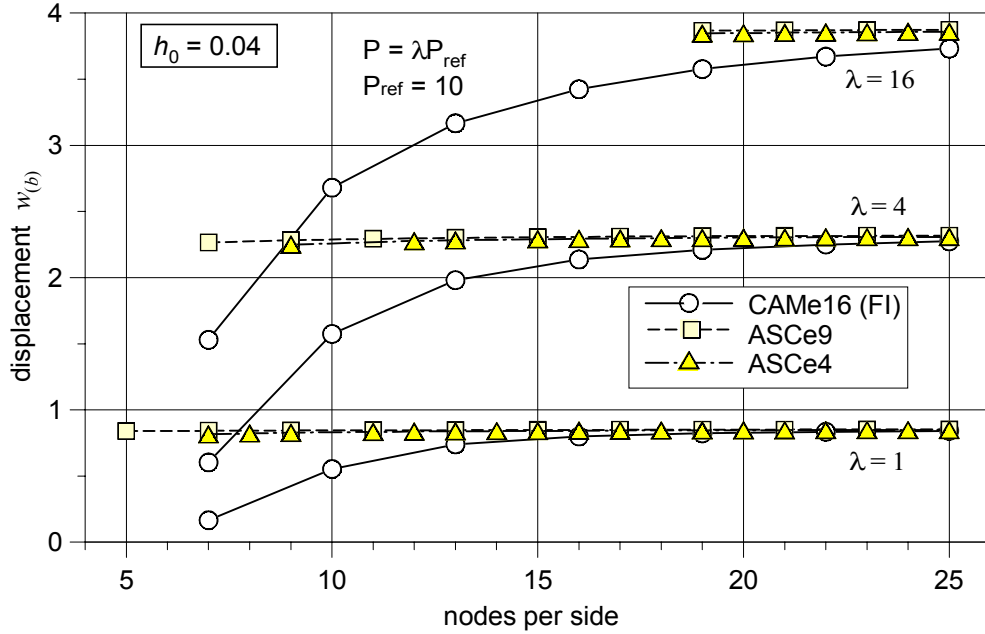


Fig. 6.12. The hemisphere with the hole: the slower rate of convergence with increasing load level

The results of our static analysis depicted in Fig. 6.11 and Fig. 6.12 are obtained using several FE formulations. Here CAM indicates the displacement-rotation-based elements, SEM – semi-mixed elements, and ASC – assumed strain elements. The notion eN after the element symbols indicates the number of nodes N in the element. Detailed description of the elements is given in [8]. The results indicate that the solution convergence becomes much slower with an increase of the range of non-linear deformation, the phenomenon not discussed in the literature and therefore ignored. It seems that there is a simple explanation for this slower rate of convergence. When the process of non-linear deformation develops, the possibilities to reproduce by the finite elements of the complex shell shapes with short wavelengths are getting worse, even with the use of the finer FE meshes.

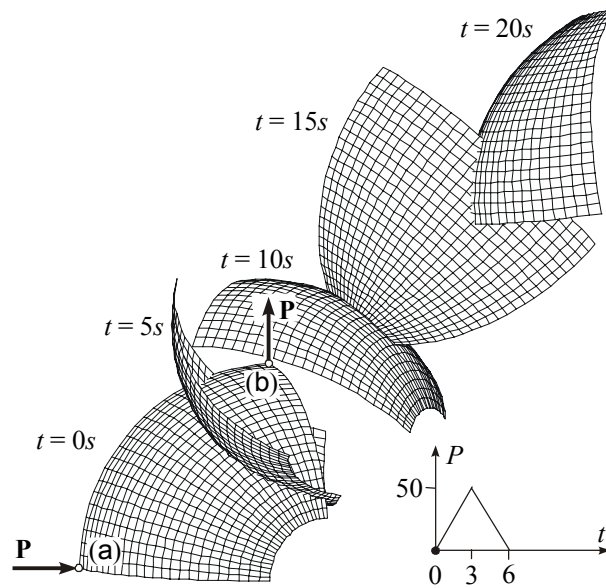


Fig. 6.13. The octant panel of the hemisphere: deformed configurations at specified time instants

In dynamic analysis of the octant panel, we free the boundary constraints and discuss its large motion as in [1]. The applied forces are now ramped from 0 to a value of 50 over 5 sec and ramped back down to 0 in another 5 sec, Fig. 6.13. Several stages of the

deformed octant panel at specified time instants are shown in Fig. 6.13, while Fig. 6.14 indicates the trajectories of the points (a) and (b) in time, projected onto the $X-Y$ coordinate plane. Fig. 6.15 contains time history plots of the potential, kinetic and total energies.

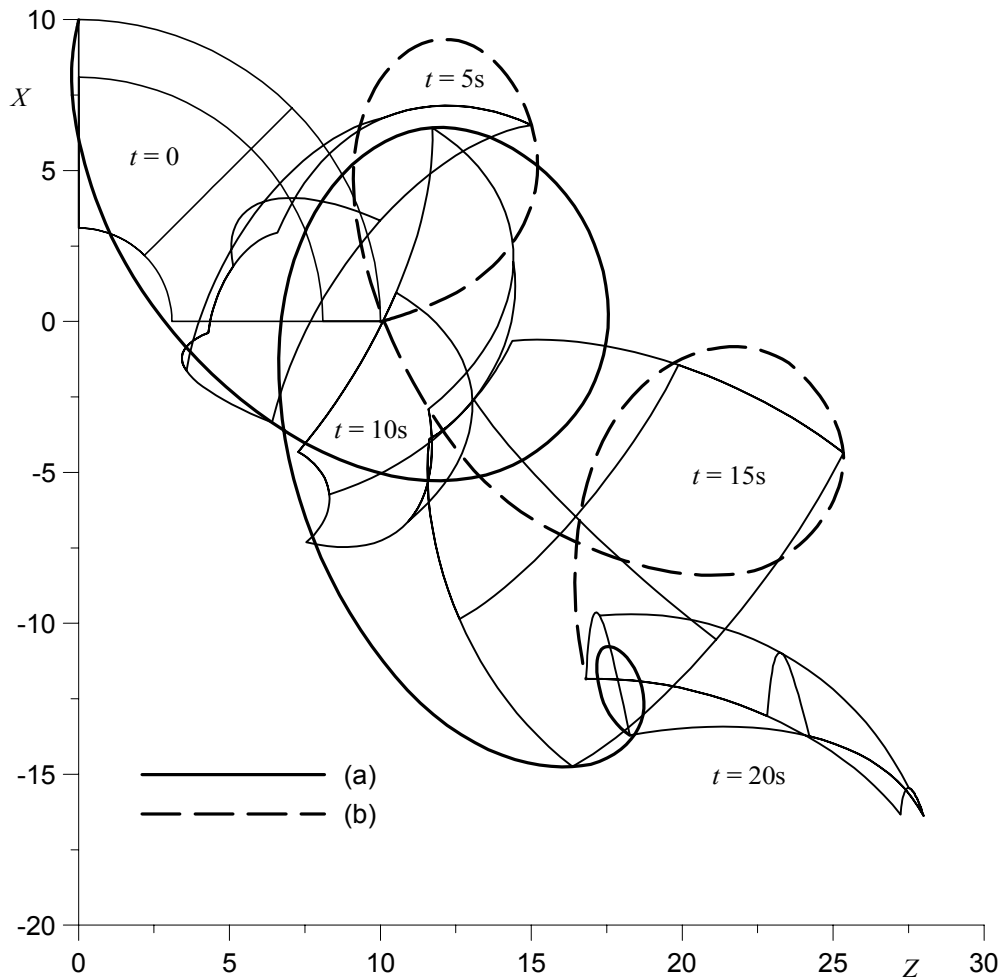


Fig. 6.14. The octant panel of the hemisphere: The trajectories of the points (a) and (b) in time

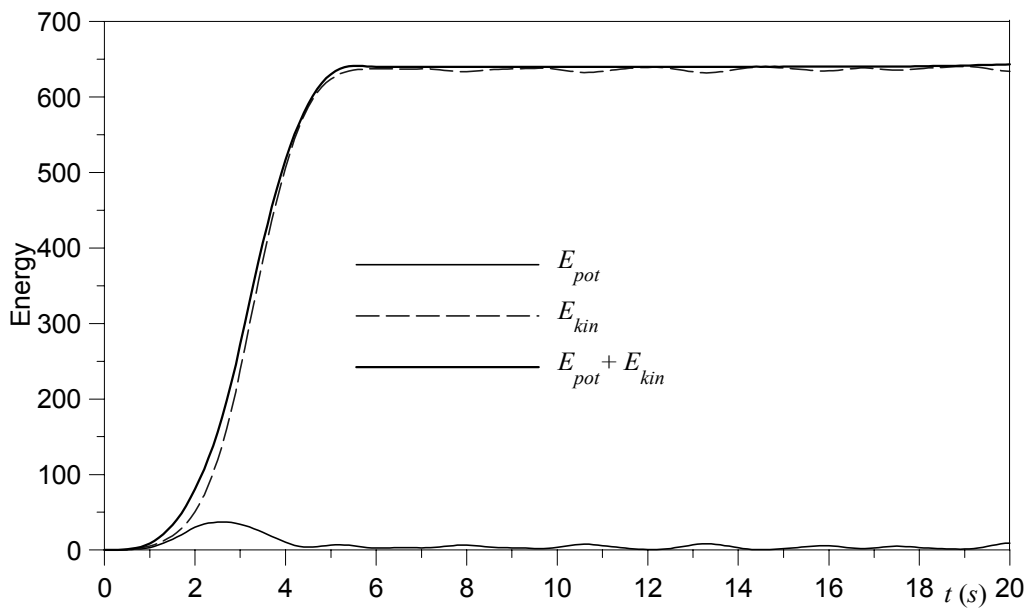


Fig. 6.15. The octant panel of the hemisphere: time history plots of energies

6.5. Large motion of a wavy cylindrical branched panel

Consider the large motion of a flexible cylindrical panel with change of the curvature sign, reinforced by a plate rib. The shell shape is indicated in Fig. 6.15, where the data have the following numerical values: $L = 2$, $\alpha = 0.4$, $R = 1$, $H = 0.4$, $h_0 = 0.01$, $E = 10^5$, $\nu = 0.25$, $\rho_0 = 100$, $\rho_0 h_0 = 1$. Two concentrated forces are applied at the points (a) and (b) by the ramp function from 0 to 10 in 1 sec and back down to 0 in another 1 sec. After the 2 sec the shell is free from external loading and moves freely in the space.

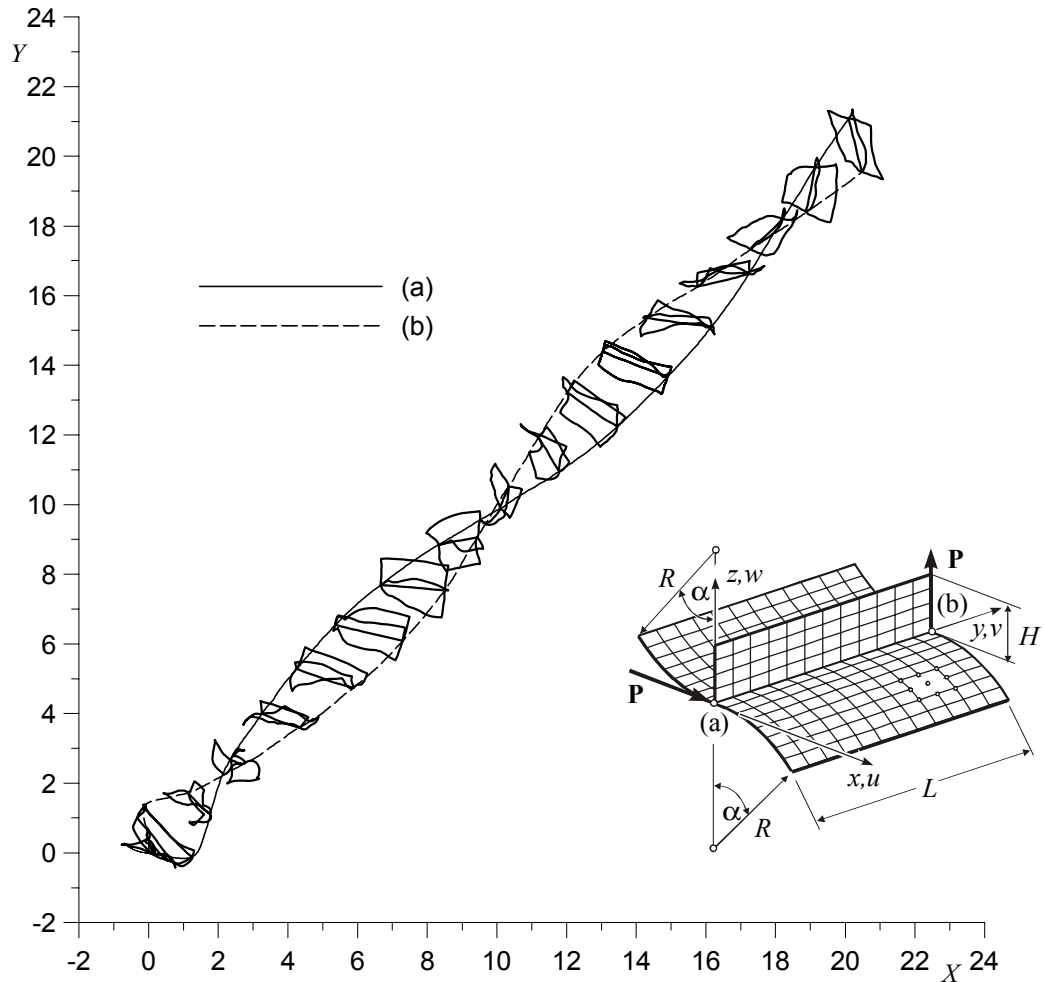


Fig. 6.15. Motion trajectories of the points (a) and (b) and the shape of the wavy cylindrical branched panel

The motion trajectories of the points (a) and (b) are shown in Fig. 6.15. Several stages of the motion depicted in Fig. 6.16 show very large deformations of the flexible shell structure. The energy histories given in Fig. 6.17 indicate that the total energy is conserved throughout the simulation time.

7. Conclusions

In this report we have tested the general six-field theory of branched shell structures developed in [6-10] on various non-linear problems of shell dynamics involving also the large overall motion. With four parameters, our dynamic algorithm can be adjusted to a variety of time-stepping schemes. We have discussed an accurate, indirect C^0 interpolation procedure on $SO(3)$ with a transport of approximation domain. The procedure has allowed

us to solve problems with unbounded rotations. Several dynamic simulations of the 2D and 3D large overall motions of various beam and shell structures have been performed. The numerical results confirm that our shell model and the time-stepping algorithm can successfully be applied to simulate highly non-linear problems of dynamic behaviour of the complex shell structures.

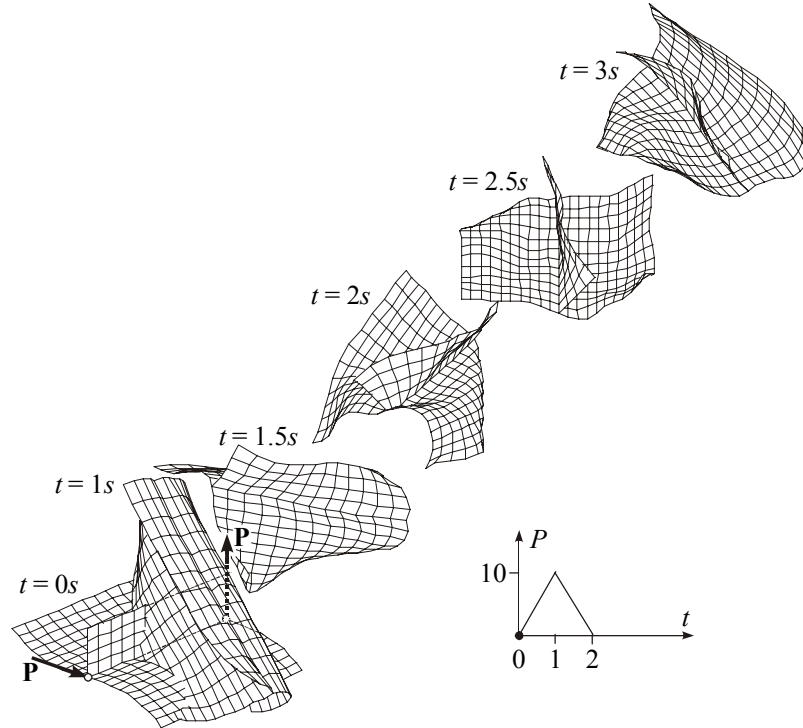


Fig. 6.16. Deformed configurations in time of the wavy cylindrical branched panel

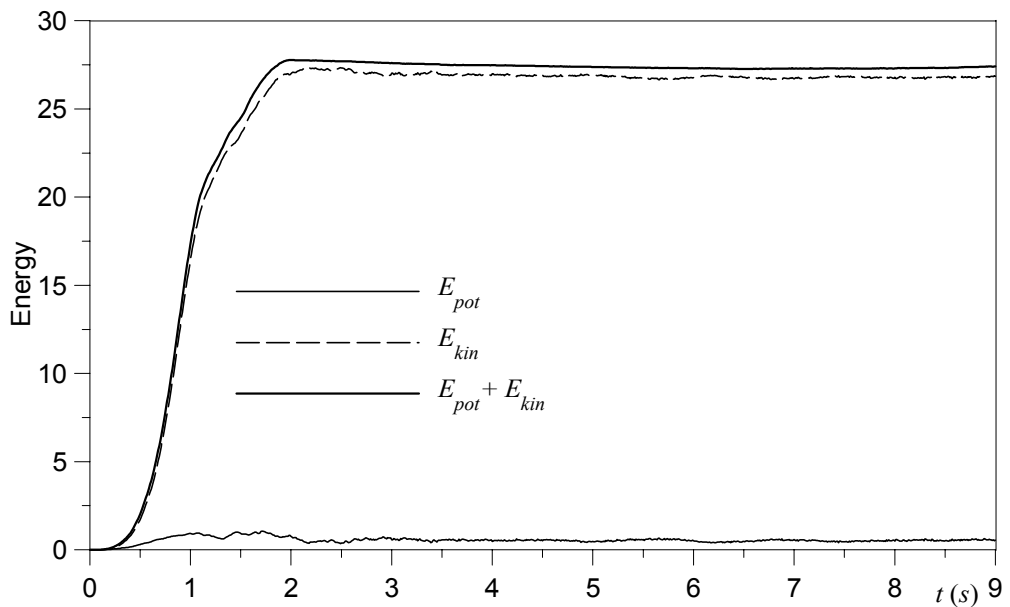


Fig. 6.17. Energy histories for the wavy cylindrical branched panel

Acknowledgements. This work was supported by the Polish State Committee for Scientific Research under grants No 7 T07A 021 12 and No 7 T07A 021 16.

References

- [1] J.C. Simo, M.S. Rifai and D.D. Fox, On a stress resultant geometrically exact shell model. Part VI: Conserving algorithms for non-linear dynamics, *International Journal for Numerical Methods in Engineering* **34** (1992) 117-164.
- [2] J.C. Simo and N. Tarnow, A new energy and momentum conserving algorithm for the non-linear dynamics of shells, *International Journal for Numerical Methods in Engineering* **37** (1994) 2527-2549.
- [3] D. Kuhl and E. Ramm, Constraint energy momentum algorithm and its application to non-linear dynamics of shells, *Computer Methods in Applied Mechanics and Engineering* **136** (1996) 293-315.
- [4] E. Madenci and A. Barut, Dynamic response of thin composite shells experiencing non-linear elastic deformations coupled with large and rapid overall motions, *International Journal for Numerical Methods in Engineering* **39** (1996) 2695-2723.
- [5] B. Brank, L. Briseghella, N. Tonello and F.B. Damjanic, On non-linear dynamics of shells: Implementation of energy-momentum conserving algorithm for a finite rotation shell model, *International Journal for Numerical Methods in Engineering* **42** (1998) 409-442.
- [6] J.G. Simmonds, The nonlinear thermodynamical theory of shells: descent from 3-dimensions without thickness expansion. In: E.L. Axelrad and F.A. Emmerling (eds.), *Flexible Shells, Theory and Applications*. Springer-Verlag, Berlin, 1984, pp. 1-11.
- [7] J. Chróścielewski, J. Makowski and H. Stumpf, Genuinely resultant shell finite elements accounting for geometric and material non-linearity, *International Journal for Numerical Methods in Engineering* **35** (1992) 63-94.
- [8] J. Chróścielewski, Rodzina elementów skończonych klasy C^0 w nieliniowej sześcioparametrowej teorii powłok, *Zeszyty Naukowe Politechniki Gdańskiej* Nr 540, *Budownictwo Lądowe* **LIII** (1996) 1-291.
- [9] J. Chróścielewski, J. Makowski and H. Stumpf, Finite element analysis of smooth, folded and multi-shell structures, *Computer Methods in Applied Mechanics and Engineering* **141** (1997) 1-46.
- [10] A. Libai and J.G. Simmonds, *The Nonlinear Theory of Elastic Shells*, 2nd ed. Cambridge University Press, Cambridge 1998.
- [11] D. Kuhl and M.A. Crisfield., Energy-conserving algorithms in non-linear structural dynamics, *International Journal for Numerical Methods in Engineering* **45** (1999) 569-599.
- [12] J.C. Simo and L. Vu-Quoc, On the dynamics in space of rods undergoing large motions a geometrically exact approach, *Computer Methods in Applied Mechanics and Engineering* **66** (1988) 125-161.
- [13] C. Cardona and M. Geradin, A beam finite element non-linear theory with finite rotations, *International Journal for Numerical Methods in Engineering* **26** (1988) 2403-2438.
- [14] J.C. Simo and K.K. Wong, Unconditionally stable algorithms for rigid body dynamics that exactly preserve energy and momentum, *International Journal for Numerical Methods in Engineering* **31** (1991) 19-52.
- [15] J. Makowski, W. Pietraszkiewicz and H. Stumpf, Jump conditions in the non-linear theory of thin irregular shells, *Journal of Elasticity* **54** (1999) 1-26.
- [16] N.N. Newmark, A method of computation for structural dynamics, *Journal of the Engineering Mechanics Division, Proc. ASCE* **85** (1959) 67-94.
- [17] J. Chung and G.M. Hulbert, A time integration algorithm for structural dynamics with improved numerical dissipation: the generalised α – method, *Journal of Applied Mechanics, Trans. ASME* **60** (1993) 371-375.
- [18] O.C. Zienkiewicz, *The Finite Element Method in Engineering Science*, 2nd ed. McGraw-Hill, London, 1971.
- [19] J. Chróścielewski, J. Makowski and W.M. Smoleński, On the interpolation in the $SO(3)$ group, in *Proc. XI Polish Conf. on Computer Methods in Mechanics*, Kielce 1993, Vol. **I**, 187-194.
- [20] M.A. Krasnosel'skii, G.M. Vainikko, P.P. Zabreiko, Ya.B. Rutitskii and V.Ya. Stetsenko, *Approximate Solutions of Operator Equations*. Wolters-Noordhoff Pub., Groningen, 1972.